TITLE:

A Heterothermic Kinetic Model of Hydrogen Absorption in Metals with Subsurface Transport

AUTHOR(S):

Ono, Shunsuke; Uchikoshi, Takeru; Hayashi, Yusuke; Kitagawa, Yuta; Yeh, George; Yamaguchi, Eiichi; Tanabe, Katsuaki

metals

MDPI

Article

A Heterothermic Kinetic Model of Hydrogen Absorption in Metals with Subsurface Transport

Shunsuke Ono [1], Takeru Uchikoshi [1], Yusuke Hayashi [1], Yuta Kitagawa [1], George Yeh [1,2], Eiichi Yamaguchi [3] and Katsuaki Tanabe [1,*]

[1] Department of Chemical Engineering, Kyoto University, Nishikyo, Kyoto 615-8510, Japan
[2] Department of Chemical Engineering, University of Manchester, Oxford Rd, Manchester M13 9PL, UK
[3] Graduate School of Advanced Integrated Studies in Human Survivability, Kyoto University, Sakyo, Kyoto 606-8306, Japan
* Correspondence: tanabe@cheme.kyoto-u.ac.jp

check for updates

Abstract: A versatile numerical model for hydrogen absorption into metals was developed. Our model addresses the kinetics of surface adsorption, subsurface transport (which plays an important role for metals with active surfaces), and bulk diffusion processes. This model can allow researchers to perform simulations for various conditions, such as different material species, dimensions, structures, and operating conditions. Furthermore, our calculation scheme reflects the relationship between the temperature changes in metals caused by the heat of adsorption and absorption and the temperature-dependent kinetic parameters for simulation precision purposes. We demonstrated the numerical fitting of the experimental data for various Pd temperatures and sizes, with a single set of kinetic parameters, to determine the unknown kinetic constants. Using the developed model and determined kinetic constants, the transitions of the rate-determining steps on the conditions of metal-hydrogen systems are systematically analyzed. Conventionally, the temperature change of metals during hydrogen adsorption and absorption has not been a favorable phenomenon because it can cause errors when numerically estimating the hydrogen absorption rates. However, by our calculation scheme, the experimental data obtained under temperature changing conditions can be positively used for parameter fitting to efficiently and accurately determine the kinetic constants of the absorption process, even from a small number of experimental runs. In addition, we defined an effectiveness factor as the ratio between the actual absorption rate and the virtually calculated non-bulk-diffusion-controlled rate, to evaluate the quantitative influence of each individual transport process on the overall absorption process. Our model and calculation scheme may be a useful tool for designing high-performance hydrogen storage systems.

Keywords: hydrogen; hydride; metal; palladium; absorption; adsorption; diffusion; storage; modelling; heat

1. Introduction

Understanding the kinetics of the hydrogen transport processes on the surface of and inside of metals is essential for manufacturing practical solid-state hydrogen storage devices based on hydrogen-absorbing metals and alloys [1–3]. Modeling the kinetics of the hydrogen absorption processes to numerically simulate the absorption rates for different conditions would be useful for efficiently designing and optimizing high-performance hydrogen storage systems.

Figure 1 illustrates the basic concept of hydrogen absorption by metals [4,5]. First, gaseous hydrogen molecules dissociate into atoms at the metal surface and then the atoms are adsorbed on the surface sites. The hydrogen atoms are transported from the surface sites to the subsurface sites,

and then to the bulk region where they diffuse. A region known as *subsurface* has been identified and defined in the literature [4–6]. The subsurface is the region located at the transition from the surface area to the bulk region of a material. The subsurface typically consists of one or two atomic monolayers immediately below the surface and is a different environment from both the surface and the bulk region. The potential energy profile of metals for hydrogen absorption is schematically presented in Figure 2. A difference in the activation energies of the subsurface and bulk region can be noticed.
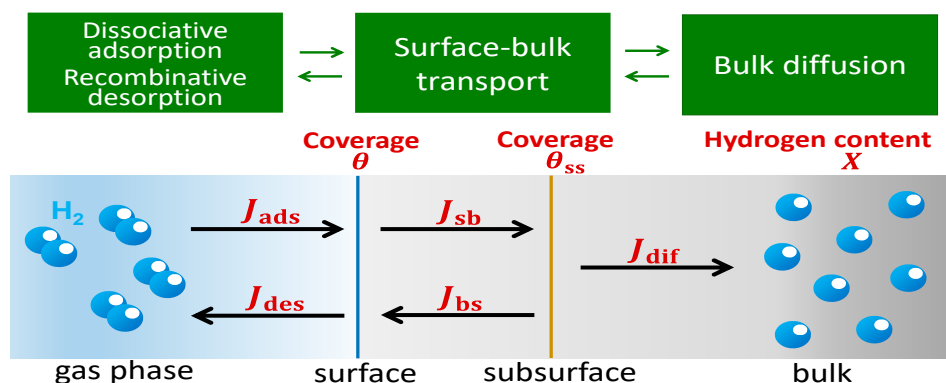

Figure 1. Conceptual schematic diagram of hydrogen absorption into metals. J_{abs} and J_{des} are the hydrogen fluxes for the surface adsorption and desorption processes, respectively; J_{sb} and J_{bs} are the fluxes for the migration of hydrogen from the surface to the subsurface, and from the subsurface to the surface, respectively; and J_{dif} is the hydrogen flux for the diffusion in the bulk region.
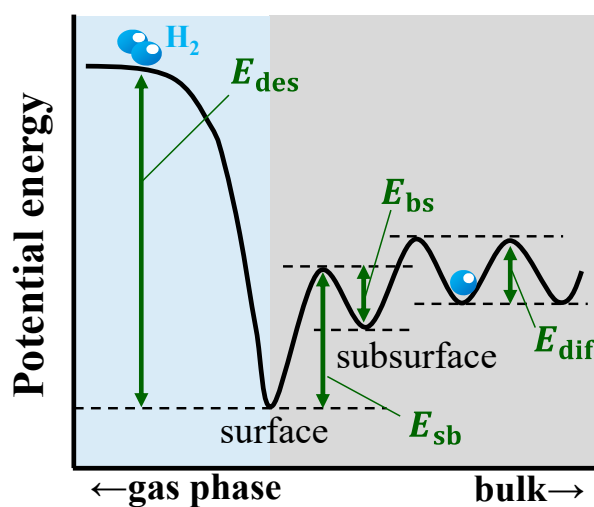

Figure 2. Schematic diagram of potential energy profile of hydrogen absorbing metals. E_{des}, E_{sb}, E_{bs}, and E_{dif} are the activation energy values for the desorption, migration of hydrogen from the surface to the subsurface and from the subsurface to the surface, and diffusion of hydrogen in the bulk region, respectively.

Research into the adsorption and desorption of hydrogen at metal surfaces has made significant progress, and the corresponding physical mechanisms for these processes have been established [7–11]. However, the behavior of hydrogen at the subsurface sites is still poorly understood [12]. Moreover, the atomic-level hydrogen absorption mechanism has not been established yet, and scientists have been debating between the penetration mechanisms, quantum tunneling, or a multi-atomic concerted process [12].

For metals featuring high surface activity for the dissociative adsorption of hydrogen molecules, such as Pd [12–15], the transport of hydrogen across the subsurface region often becomes the rate-determining process, in contrast to metals featuring lower surface activity, such as Mg [16–18].

A significant discrepancy has been frequently observed between the atomic coverage at the surface and that at the subsurface for high-surface-activity metals featuring low activation energy or potential barrier for the dissociative surface adsorption of hydrogen molecules [5,6]. Therefore, the hydrogen transport across the subsurface should be taken into account when developing numerical models that would be used for highly accurate simulations of the net absorption rates of high-surface-activity metals. In addition, temperature changes in metals during hydrogen absorption, owing to the heat of adsorption and absorption, could cause errors in the numerical simulations used to estimate the hydrogen absorption rates because many kinetic parameters are temperature-sensitive. Therefore, in this study, we developed a versatile kinetic model of hydrogen absorption into metals, which accounted for the subsurface transport process and temperature changes.

2. Theory and Calculation Methods

The basic concept of our calculation model is schematically depicted in Figures 1 and 2. First, gaseous hydrogen molecules dissociate into hydrogen atoms at the metal surface, then the atoms are adsorbed on the surface sites. The hydrogen atoms migrate from the surface sites to the subsurface sites and then to the bulk region where they diffuse. In the model, we accounted for the hydrogen fluxes for the surface adsorption and desorption processes, the subsurface transport between the surface and the bulk region, and the diffusion in the bulk region. The mass balances for the fractional coverages (occupancy) at the surface and subsurface (θ and θ_{ss}, respectively) and the hydrogen content X [mol-H/mol-Pd] could be expressed as follows:

$$N_s \frac{d\theta}{dt} = J_{ads} - J_{des} - J_{sb} + J_{bs}, \tag{1}$$

$$N_s \frac{d\theta_{ss}}{dt} = J_{sb} - J_{bs} - J_{dif}, \tag{2}$$

$$N_b \delta \frac{dX}{dt} = J_{sb} - J_{bs}, \tag{3}$$

where J_{abs} and J_{des} are the hydrogen fluxes for the surface adsorption and desorption processes, respectively; J_{sb} and J_{bs} are the hydrogen fluxes for the inward and outward subsurface transport, respectively; J_{dif} is the hydrogen flux for the diffusion in the bulk region; N_s (2.8×10^{-5} mol m^{-2} [19]) is the number of atomic sites per unit of surface area; N_b (1.1×10^5 mol m^{-3} [19]) is the number of atomic sites per unit of volume; and δ is the thickness of the bulk region. The J_{abs}, J_{des} [19], J_{sb}, J_{bs} [20], and J_{dif} values could be calculated as follows [19,20]:

$$J_{ads} = 2S(\theta) \frac{P_{H_2}}{\sqrt{2\pi M_{H_2} RT}}, \tag{4}$$

$$J_{des} = 2k_d{}^0 N_s{}^2 \theta_{HH} \exp\left(-\frac{2E_{des}}{RT}\right), \tag{5}$$

$$J_{sb} = k_{sb}{}^0 N_s \theta (1 - \theta_{ss}) \exp\left(-\frac{E_{sb}}{RT}\right), \tag{6}$$

$$J_{bs} = k_{bs}{}^0 N_s \theta_{ss} (1 - \theta) \exp\left(-\frac{E_{bs}}{RT}\right), \tag{7}$$

$$J_{dif} = D_H{}^0 \frac{\partial C(z,t)}{\partial z} \exp\left(-\frac{E_{dif}}{RT}\right), \tag{8}$$

where S is the capturing coefficient; P_{H2} and M_{H2} are the partial pressure and molar mass of hydrogen, respectively; R and T are the ideal gas constant and absolute temperature, respectively; $k_d{}^0$ (4.8×10^{17} m^2 mol^{-1} s^{-1} [19]), $k_{sb}{}^0$, and $k_{bs}{}^0$ are the frequency factors for the surface desorption and the inward and outward subsurface transport of hydrogen atoms, respectively; E_{des} (4.2×10^4 J mol^{-1} [19]), E_{sb}

(5.6×10^4 J mol^{-1} [20]), E_{bs} (2.2×10^4 J mol^{-1} [20]), and E_{dif} (2.2×10^4 J mol^{-1} [20]) are the activation energy values for the desorption, inward and outward subsurface transport, and diffusion of hydrogen in the bulk region, respectively; $D_{\text{H}}{}^0$ (2.9×10^{-7} m^2 s^{-1} [20]) is the pre-factor of diffusion coefficient of hydrogen; and C is the local concentration of hydrogen in the bulk region. Two adjacent vacant surface atomic sites are required for the dissociative surface adsorption of hydrogen molecules. Similarly, two adjacent occupied surface sites are required for the recombinative surface desorption of hydrogen atoms. Therefore, we rigorously accounted for the locations of the adsorption and desorption sites on the surface, as follows [19,21]:

$$\theta_{OO} = 1 - \theta - \frac{\theta_{OH}}{2}, \tag{9}$$

$$\theta_{HH} = \theta - \frac{\theta_{OH}}{2}, \tag{10}$$

where θ_{OO} and θ_{HH} are the probabilities that two adjacent sites are both vacant or occupied, respectively, and θ_{OH} is the probability that one of two adjacent sites is vacant. Assuming that θ_{OO}, θ_{HH}, and θ_{OH} reach chemical equilibrium, the following equation has been proposed [19,21]:

$$\frac{4\theta_{OO}\theta_{HH}}{\theta_{OH}{}^2} = \exp\left(-\frac{E_{eq}}{RT}\right), \tag{11}$$

where E_{eq} (2.1×10^3 J mol^{-1} [19]) is the energy separation between the site-occupation states. From Equations (9)–(11), θ_{OO} and θ_{HH} can be expressed as:

$$\theta_{OO} = 1 - \theta - \frac{2\theta(1-\theta)}{1 + \sqrt{1 - 4\theta(1-\theta)\left\{1 - \exp\left(-\frac{E_{eq}}{RT}\right)\right\}}}, \tag{12}$$

$$\theta_{HH} = \theta - \frac{2\theta(1-\theta)}{1 + \sqrt{1 - 4\theta(1-\theta)\left\{1 - \exp\left(-\frac{E_{eq}}{RT}\right)\right\}}}. \tag{13}$$

The capturing coefficient, $S(\theta)$, which takes into account the hopping of the physisorbed hydrogen molecules at the surface, can be expressed as follows [19,21]:

$$S(\theta) = \frac{S_0}{1 + K\left(\frac{1}{\theta_{OO}} - 1\right)}, \tag{14}$$

where S_0 is the capturing coefficient for $\theta = 0$, which we set to be 1.0 (dimensionless) [21] in this study, and K (5.0×10^{-2} (dimensionless) [19]) is a constant related to the surface adsorption and desorption. The value of S_0 has little influence on the calculation results in this study because of the subsurface-transport-control or bulk-diffusion-control nature. When fitting our calculations to the experimental data, we assumed that the adsorption and desorption at the Pd surface were always in equilibrium [19,22]. Based on the above-described model, we calculated the time evolution of the hydrogen concentration profile in Pd. We considered $k_{\text{sb}}{}^0$ and $k_{\text{bs}}{}^0$ to be the fitting kinetic parameters for the transport of hydrogen atoms between the Pd surface and subsurface, and we determined them using numerical fitting.

3. Experimental Methods

3 cm × 3 cm flat Pd plates of various thicknesses (0.2, 0.5, 1, and 2 mm) were used in this study. First, we annealed the Pd samples at 1000 °C for 10 h in a furnace under a nitrogen atmosphere to thoroughly crystallize the material and to degrease the surface for good experimental reproducibility. Then each Pd sample was placed inside a stainless steel vacuum chamber with the capacity of 1.55×10^3 cm^3. The chamber was evacuated (~10^{-8} Torr) and then hydrogen gas was promptly injected

into the chamber to reach the pressure of 760 Torr. Afterward, the pressure in the chamber gradually decreased owing to the absorption of hydrogen into Pd. The chamber pressure was monitored in time to determine the hydrogen content in Pd. The temperature of Pd was also monitored using a thermocouple. For some experimental runs, the Pd sample was actively heated using a heater to investigate the temperature dependence of the hydrogen absorption rate.

4. Results and Discussion

4.1. Hydrogen Absorption Rate at Room Temperature

4.1.1. Experimental Data and Numerical Fitting

Figure 3 presents the time evolution of the hydrogen content in a 1 mm-thick Pd sample at the initial Pd temperature of 17 °C; Pd was not actively heated. The fitting result of our model calculation is also plotted in Figure 3. For the numerical fitting, we considered k_{sb}^0 and k_{bs}^0 to be the fitting parameters, and used literature-reported values for E_{sb} and E_{bs} [20] and also for the other adsorption, desorption, and diffusion parameters [19,20]. Through numerical fitting, we determined the kinetic parameters k_{sb}^0 and k_{bs}^0 to be 5.7×10^{12} and 1.3×10^{12} s^{-1}, respectively, for the transportation of atomic hydrogen between the Pd surface and subsurface. Because a single, monotonic curve had to be fit, multiple combinations of k_{sb}^0 and k_{bs}^0 values could be used to achieve favorable fits.
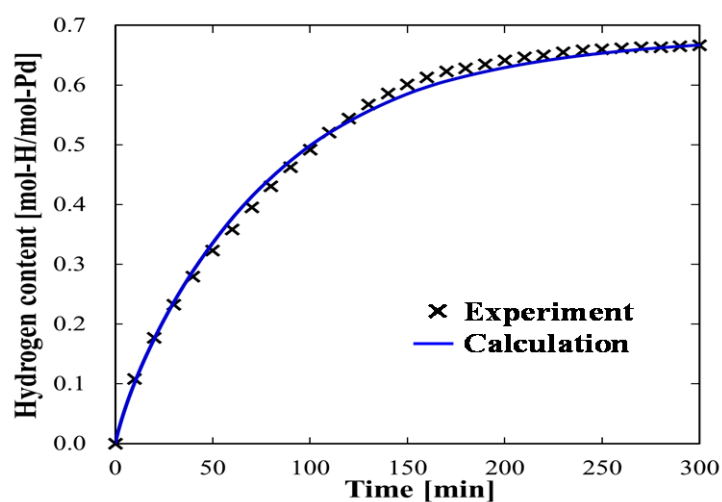

Figure 3. Experimental result and calculated fitted result of the time evolution of hydrogen content in Pd at 17 °C.

4.1.2. Case Study Simulation I: Effective Surface Area and Hydrogen Absorption Rate

After we obtained the kinetic parameters, we were able to perform simulations. Herein, we included some case studies to demonstrate the usefulness of our numerical model. First, we increased the hydrogen absorption rate by increasing the effective surface area of the metals using a roughening surface treatment, such as chemical wet etching. Figure 4 presents the simulation results for hydrogen absorption using 1 mm-thick Pd plates of various effective surface areas. As the effective surface area increased, the hydrogen absorption rate increased. However, the degree of increment decreased as the surface area continued to increase. This tendency could be attributed to the changes in the hydrogen flux. During the initial absorption stage, as the effective surface area increased, the hydrogen flux significantly increased. However, the flux gradually decreased as the bulk diffusion slowed owing to the decrease in the hydrogen-concentration slope particularly around the central region of Pd. From these simulation results, we concluded that to increase the hydrogen absorption rate, it would be effective to achieve an effective surface area several times larger than that of the smooth surface Pd.

Moreover, the simulation results indicated that, to further increase the hydrogen absorption rate, it would be advantageous to decrease the influence of the bulk diffusion.
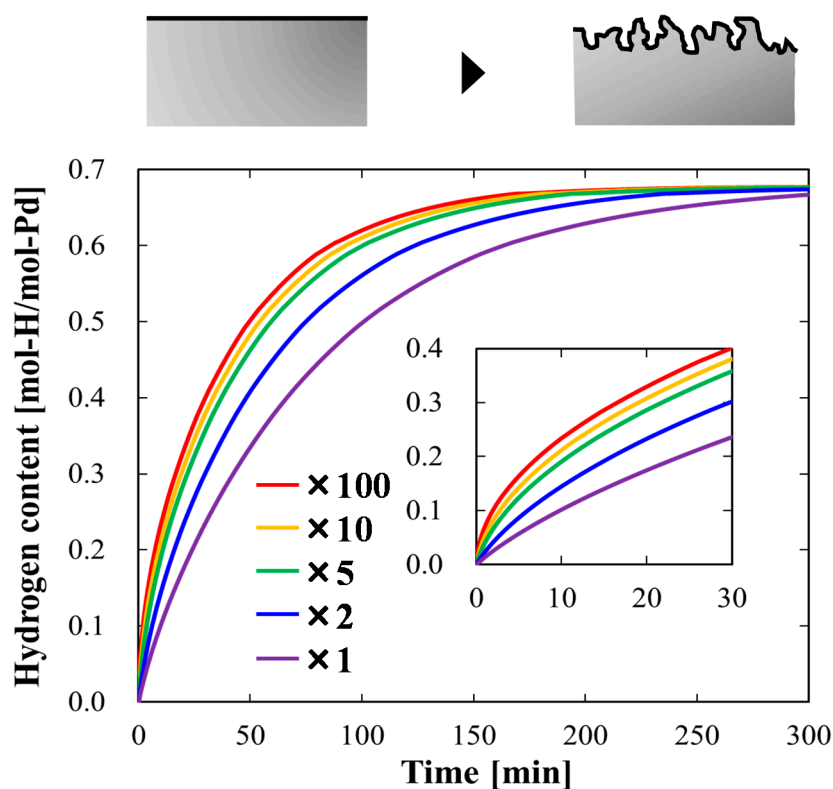

Figure 4. Simulated time evolution plots of hydrogen content absorbed in Pd plates of various effective surface areas, which were 1, 2, 5, 10, and 100 times larger than that of the smooth surface Pd. The inset depicts a magnified view for the first 30 min of the hydrogen absorption process. The accompanying schematic (top) is a conceptual drawing of the surface roughening process.

4.1.3. Case Study Simulation II: Plate Thickness and Hydrogen Absorption Rate

Next, we considered another strategy for increasing the hydrogen absorption rate: thinning the Pd plate to decrease the effect of bulk diffusion. Figure 5 depicts the numerical simulation results for the time evolutions of the hydrogen content in Pd plates of various thicknesses. In addition, Figure 6 presents the time evolution of the spatial hydrogen concentration profiles in Pd plates of various thicknesses. As the thickness of the Pd plate decreased, the hydrogen absorption rate increased. This could be attributed to the smaller influence of bulk diffusion for the thinner Pd plates owing to the sustainability of the hydrogen concentration gradient. The amount of hydrogen distributed in the bulk regions of the 500 μm and 1 mm Pd plates significantly varied from the surface to the center of the Pd plates owing to the influence of the bulk diffusion control on the overall hydrogen transport process relative to the influence of the surface adsorption and the subsurface transport. By contrast, hydrogen was uniformly distributed in the 100 μm Pd plate owing to the small influence of bulk diffusion. Therefore, we could shift the rate-determining process in the Pd-hydrogen system from bulk diffusion to surface-to-subsurface transport by thinning the Pd plates to 100 μm.
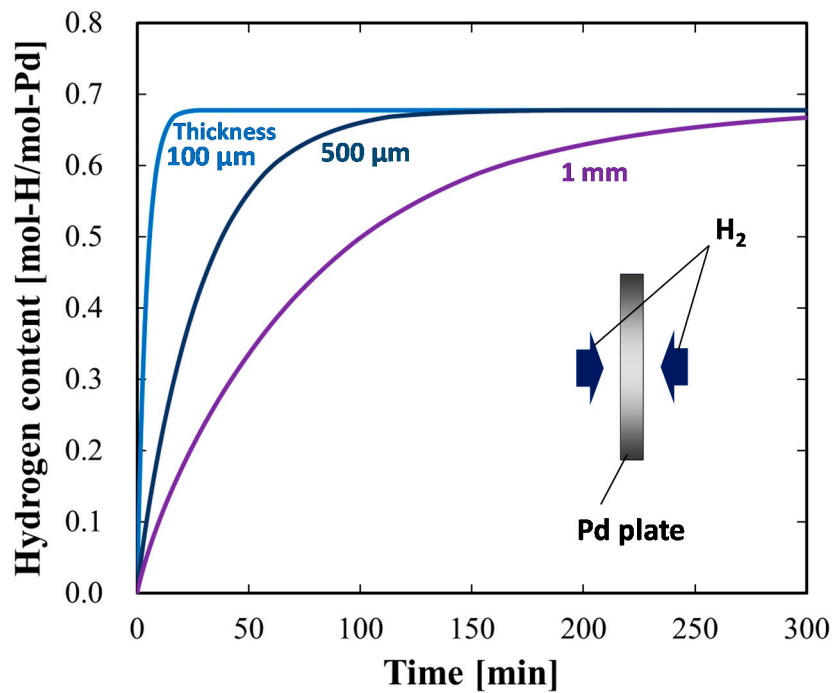
Figure 5. Simulated time evolutions of hydrogen content in Pd plates of various thicknesses.
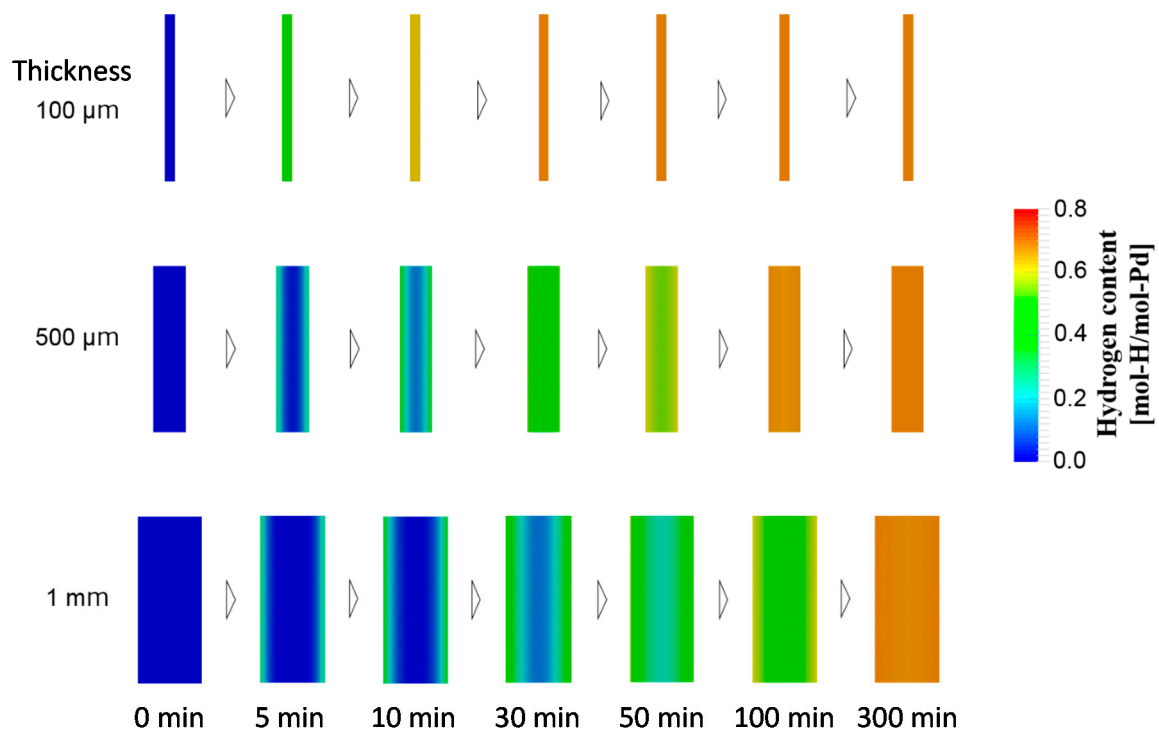

Figure 6. Spatial hydrogen concentration profiles in Pd plates at 5, 10, 30, 50, 100, and 300 min after the beginning of hydrogen absorption process for Pd plates of different thicknesses.

4.1.4. Case Study Simulation III: Particle Size and Hydrogen Absorption Rate

We considered spherical metal particles, which could be more common for practical hydrogen storage applications, in our model, and we investigated decreasing the particle size to increase the hydrogen absorption rate. For the calculations, we used the spherical form of the diffusion equation [23], instead of Equation (8). Figure 7 presents the results of the numerical simulation for the time evolution of the hydrogen content in spherical Pd particles of various diameters. Figure 8 presents the time

evolution of the spatial hydrogen concentration profiles in Pd particles of various diameters. Similarly to the plate-shaped Pd, as the diameter of the Pd particles decreased, the hydrogen absorption rate increased. This tendency was again attributed to the smaller influence of the bulk diffusion control for smaller particles. The hydrogen absorption rate was higher for the Pd particles than for the Pd plates of the same dimensions. This was attributed to the total surface area of the particles being larger than that of the plates. Similar to the Pd plates, it was determined that decreasing the particle diameter to 100 μm would circumvent diffusion control for the kinetically efficient hydrogen absorption process, as observed in the spatially uniform hydrogen concentration profile in Figure 8.
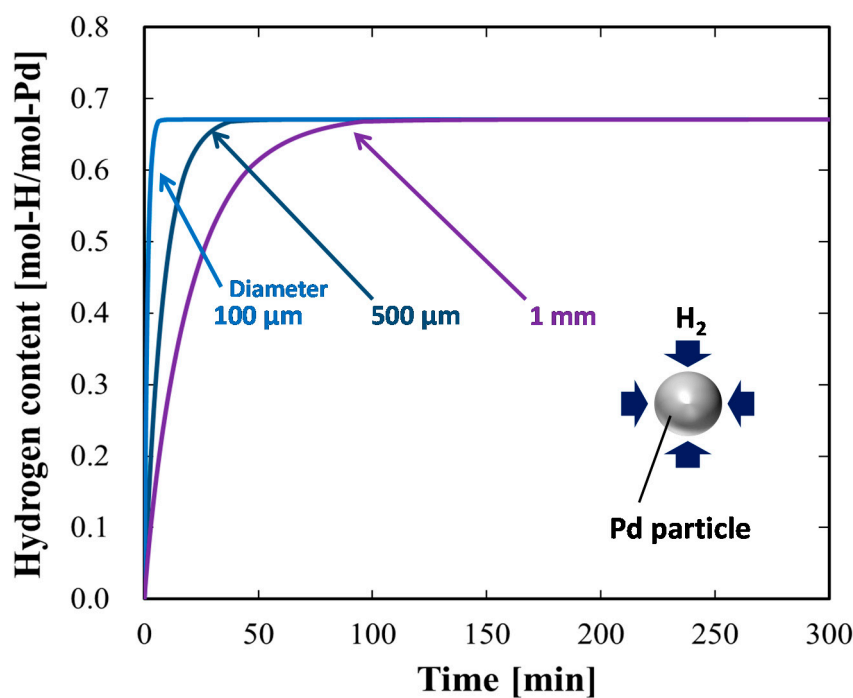

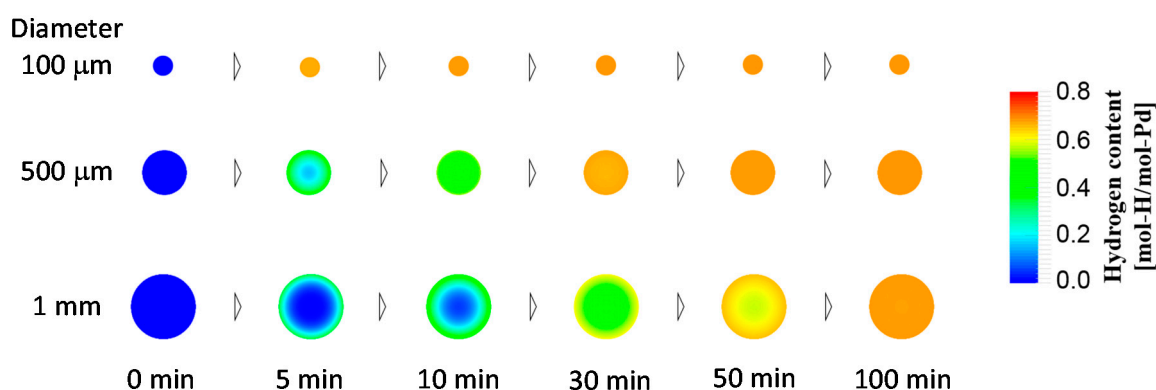**Figure 7.** Simulated time evolution of hydrogen content in spherical Pd particles of various diameters.

Figure 8. Spatial hydrogen concentration profiles in spherical Pd particles at 5, 10, 30, 50, and 100 min after the beginning of hydrogen absorption process for Pd particles of different diameters.

4.2. Hydrogen Absorption Rate at Higher Temperature

4.2.1. Heterothermic Model Development

When the Pd temperature was higher, the initial hydrogen absorption rate was high, which caused the Pd temperature to significantly increase owing to exothermic adsorption and absorption processes, as described below. When adsorption and absorption occur at high temperature, temperature evolution

in metals has to be accounted for in the numerical simulation model. To address the temperature change in metals, as we have previously conceptually proposed [24], we added a calculation routine to our kinetic model where the Pd temperature was monitored at each time step of the process, as reflected in the computation of the series of kinetic parameters illustrated in Figure 9. We updated the Pd and gas phase temperatures for each time step after using the mass balance to calculate status parameters, such as the surface coverage and hydrogen concentration for each spatial mesh. One might think that temperature evolution could be calculated using the adsorption and absorption enthalpies without utilizing the monitored temperature values. However, such calculations would require that the heat dissipation rates of the Pd samples for the heat diffusion, convection, and radiation components under non-steady-state conditions be determined. This would be a challenging approach and therefore we adopted the monitoring scheme in this study. In addition, for the experimental data reported hereafter, we have artificially modified the onset hydrogen content in such a way that the temporally saturated value equaled the literature-reported equilibrium value for Pd [25]; this should cover the initial fast uptake that was potentially missed while monitoring the pressure.
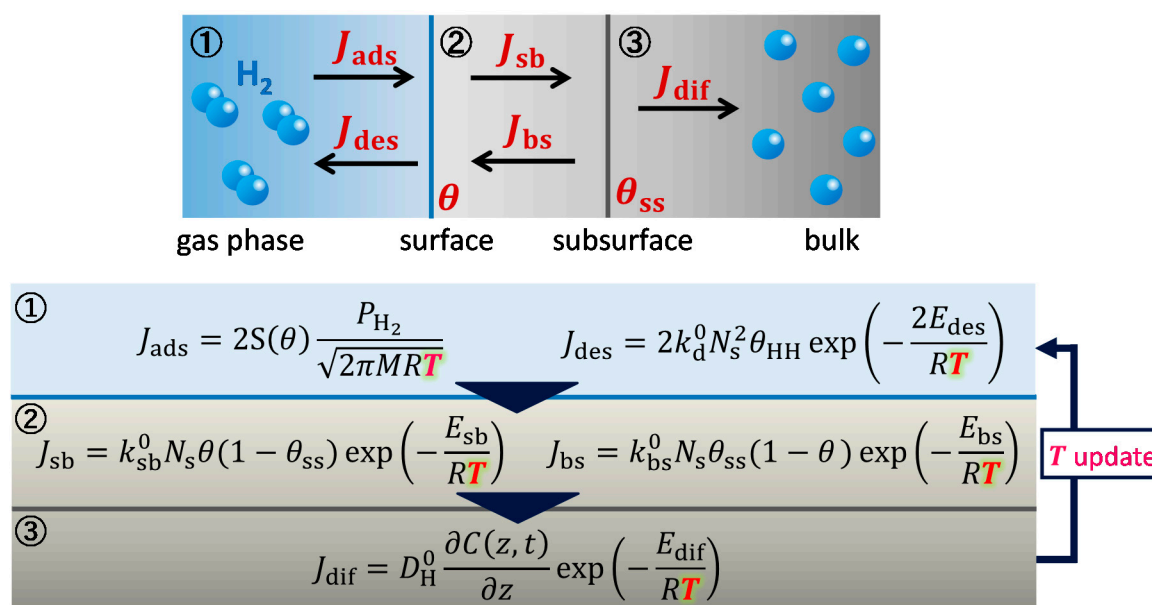

Figure 9. Summary of calculation routine accounting for temperature changes in metals.

4.2.2. Calibration of Gas Phase Temperature

Once hydrogen absorption into Pd started, the gas phase (hydrogen, in this study) temperature would no longer be equal to or at equilibrium with the measured temperature of Pd. To precisely determine the hydrogen content in Pd from the measured chamber pressure, the spatially averaged hydrogen temperature was required. Therefore, as a preparatory experiment, the chamber pressure was measured when a 1 mm-thick Pd sample was heated. In advance of this preparatory experiment, hydrogen was absorbed by the Pd sample until equilibrium was reached. When the Pd temperature increased, a certain amount of hydrogen would be desorbed owing to the decrease in the equilibrium hydrogen content in Pd [19]. To account for this effect, we estimated the gas temperature, T_{gas}, using the initial pressure and temperature, P_0 and T_0, respectively, as:

$$T_{gas}(t) = \frac{n_{H,0}}{n_{H,0} + \left\{X_0 - X_{eq}(T_{Pd}(t))\right\}n_{Pd}/2} \frac{P(t)}{P_0}T_0, \tag{15}$$

where $n_{H,0}$ is the initial number of moles of hydrogen in gas phase; X_0 and X_{eq} are the initial and equilibrium [25] hydrogen contents in Pd, respectively; T_{Pd} is the temperature of Pd; n_{Pd} is the number

of moles of Pd; and P is the temporally monitored pressure in the chamber. The time evolutions of the experimentally measured P and T_{Pd}, and estimated T_{gas} values are plotted in Figure 10. Then, the relationship between T_{gas} and T_{Pd} is presented in Figure 11. By using quadratic fitting, the following numerical relationship between T_{gas} and T_{Pd} was established to precisely determine the hydrogen content evolution and thus the hydrogen absorption rate:

$$T_{gas}\left[^{\circ}C\right] = 0.004366118 T_{Pd}{}^{2} - 0.1198489 T_{Pd} + 25.48853. \tag{16}$$
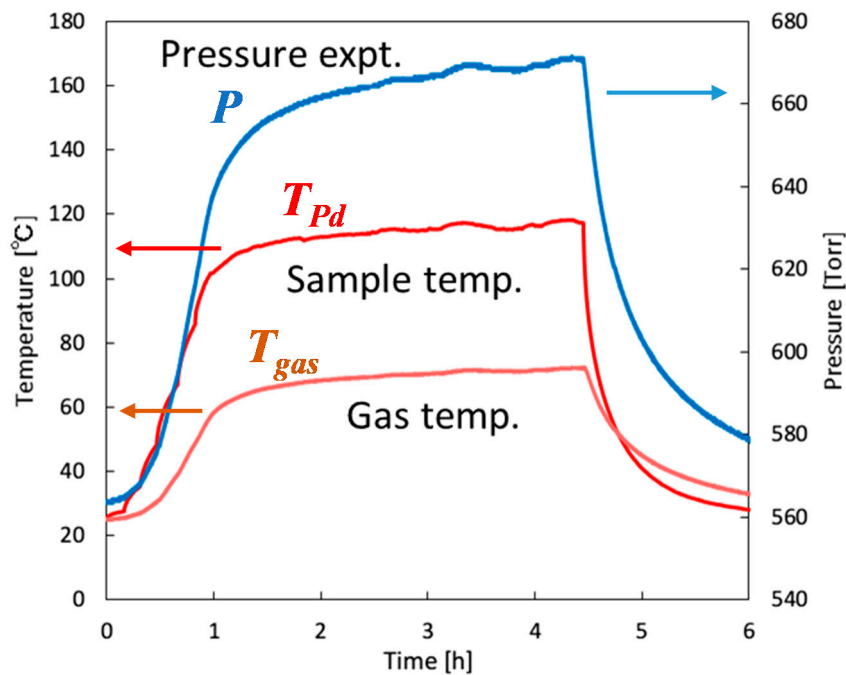

Figure 10. Time evolution of measured Pd temperature, gas phase pressure, and numerically determined gas phase temperature.
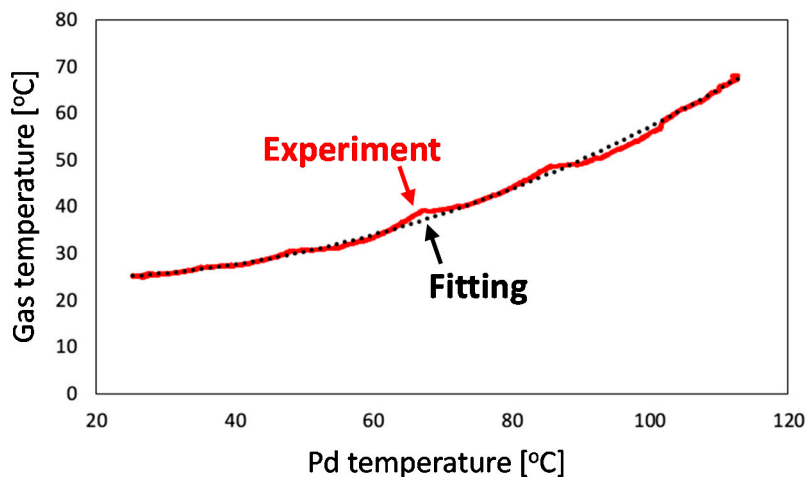

Figure 11. Relationship between Pd and gas phase temperatures.

4.2.3. Experiments and Calculations at Various Temperatures

We performed hydrogen absorption experiments at various Pd temperatures to test the heterothermic kinetic model we developed. Figure 12 presents the time evolutions of the hydrogen content in 1 mm-thick Pd samples of various initial temperatures and also the fitting results from our model calculations. Using

numerical fitting, we determined that $k_{sb}^0 = 5.8 \times 10^{12}$ s^{-1} and $k_{bs}^0 = 7.6 \times 10^{11}$ s^{-1}. We employed this single set of values of the parameters k_{sb}^0 and k_{bs}^0 for all of the following calculations. The discrepancy for the initial stage of hydrogen absorption between the experimental and numerical results, particularly for the higher temperatures, can be partly attributed to the initial fast uptake that was potentially missed while monitoring the pressure.
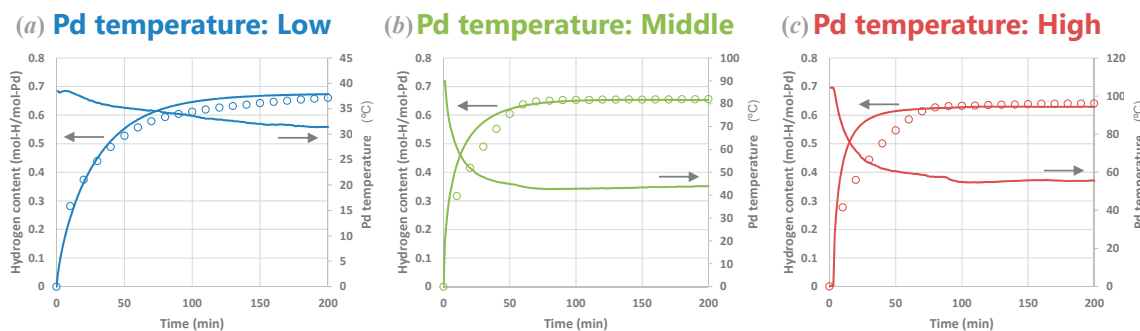

Figure 12. Experimental results (blank circles) and numerical fitting (solid lines) of time evolution of hydrogen content in Pd at different temperatures (*a*: low, *b*: middle, and *c*: high temperature ranges). The fitting parameters were $k_{sb}^0 = 5.8 \times 10^{12}$ s^{-1} and $k_{bs}^0 = 7.6 \times 10^{11}$ s^{-1} for all the calculations.

4.2.4. Experiments and Calculations for Various Metal Sizes

We tested the validity of our model and the k_{sb}^0 and k_{bs}^0 fitting parameters reported in the previous section by comparing the experimental data with the calculation results for various metal sizes. Figure 13 presents the time evolutions of the hydrogen content in Pd samples of various plate thicknesses (Pd was not actively heated) and also the fitting results from our model calculations. The discrepancy for the initial stage of hydrogen absorption between the experimental and numerical results, particularly for the thinner Pd samples, can be, again, partly attributed to the initial fast uptake that was potentially missed while monitoring the pressure. Nevertheless, the time constants for the absorption process were well reproduced for all the thicknesses using a single set of modelling parameters.
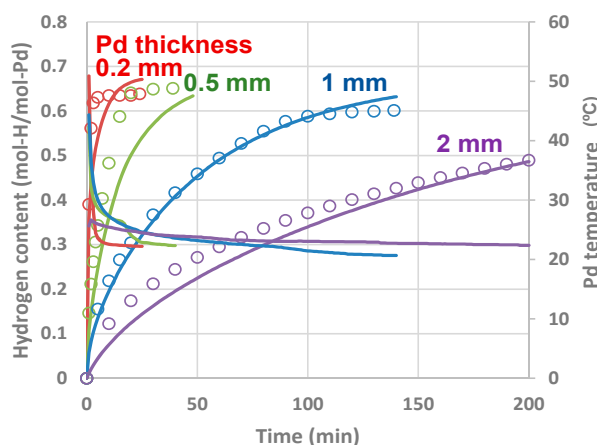

Figure 13. Experimental results (blank circles) and calculation fittings (solid lines) of time evolution of hydrogen content in Pd plates of various thicknesses. The single set of parameters $k_{sb}^0 = 5.8 \times 10^{12}$ s^{-1} and $k_{bs}^0 = 7.6 \times 10^{11}$ s^{-1} was used for all the calculations.

In Figures 12 and 13, we have demonstrated the numerical calculations fitted a series of hydrogen absorption experimental data for different temperatures and Pd sizes using a single set of material parameters. In another point of view, we have been able to finely extract the unknown kinetic parameters using the series of fittings. For the conventional Arrhenius plot scheme, multiple experimental runs at various temperatures are required. Moreover, metal temperature is not stable during the experimental

runs owing to the heat of adsorption and absorption, which is not favorable for the Arrhenius plots. Our model could provide a precise method for determining unknown parameters using the numerical fitting of the experimental data for the time evolution of the hydrogen absorption rate even from a small number of experimental runs by positively utilizing the change in temperature of the hydrogen-absorbing media; this could subsequently enable highly accurate numerical simulations. Using our calculation scheme, one can determine the temperature-dependent rate constants, including the reaction activation energy, utilizing data fitting. This would be similar to using the Arrhenius plot method but it would only require a single experimental run where the temperature would spontaneously vary owing to the exothermic adsorption and absorption processes. In addition, while we used Pd as the hydrogen-absorbing medium in this study, our numerical model could be applied to various types of metal/alloy-hydrogen systems.

4.3. Analysis of Rate-Determining Steps

Using numerical investigations in conjunction with experimental data, we have determined the kinetic parameters of the hydrogen absorption process. In this section, we use the results to analyze the rate-determining steps of the overall hydrogen transport process. We define the effectiveness factor, η, as the ratio of the actual hydrogen absorption rate to the virtually calculated non-bulk-diffusion-controlled hydrogen absorption rate. The η factor would enable us to quantitatively evaluate the influence of each transportation process and determine the rate-determining step for different metal species and structures (e.g., sizes and shapes). Figure 14 depicts the concept of the hydrogen absorption rate vs. the hydrogen content plots for the actual absorption rate, which accounted for the bulk diffusion process, and the virtually calculated absorption rate assuming sufficiently fast bulk diffusion. The hydrogen absorption rate decreased linearly as the hydrogen content increased throughout the entire hydrogen content range for the non-bulk-diffusion-control case. This occurred because in such a surface-adsorption-control or subsurface-transport-control regime, the surface or subsurface coverage becomes approximately proportional to the hydrogen content, while the adsorption or subsurface-transport rate is approximately proportional to the surface or subsurface vacancy fraction, respectively. By contrast, the relationship between the actual absorption rate and hydrogen content becomes linear in the high-hydrogen-content range because in such a bulk-diffusion-control regime the hydrogen concentration gradient approximately linearly decreases as the hydrogen content increases owing to the quasi-steady state of diffusion. Therefore, the ratio between the actual and virtual rates becomes approximately constant in the high-hydrogen-content range. For practical applications, the total hydrogen absorption duration is mainly dominated by the duration of the absorption process in the high-hydrogen-content range, where the absorption rate becomes lower and therefore the process requires more time. Therefore, it would be important to analyze the rate-determining steps, particularly in the high-hydrogen-content range. Consequently, we defined η as the ratio of the actual rate to the virtual, non-bulk-diffusion-controlled rate for the range when the hydrogen content exceeds 0.4, where η becomes constant.

Figure 15 presents the calculated η values of the Pd plates and spherical Pd particles of various thicknesses and diameters, respectively, under the constant hydrogen pressure values of 1 and 1000 atm. As the size of the Pd plates and particles decreased, η approached unity, which indicated that the process was subsurface-transport controlled. In general, a high-η state corresponds to a surface-adsorption or subsurface-transport controlled process, but in this study it was always subsurface-transport controlled owing to the high surface activity of Pd. When the plate thickness or particle diameter was smaller than 100 μm, the influence of bulk diffusion could be neglected, which was consistent with the results in Figures 5–8. Conversely, when the Pd size increased, η decreased and the hydrogen transport kinetics of the H-Pd system became bulk-diffusion controlled. The η values of the spherical Pd particles were larger than those of the Pd plates of the same sizes because of the larger specific surface area (surface area-to-volume ratio) of the particulates. In addition, the η values were higher at higher hydrogen pressure levels. Nevertheless, the differences in the η values were not significant despite

the 1000-fold increase in pressure. This was attributed to the surface adsorption rate, which is highly influenced by the hydrogen pressure, being sufficiently high compared with the subsurface-transport and bulk-diffusion rates, even at 1 atm in the high-hydrogen-content region, and therefore the effect of the hydrogen pressure on η was not significant. In this way, using η, one can quantitatively evaluate the influence of the bulk diffusion on the entire hydrogen transport process in metals and also identify the rate-determining step of the system for different conditions.
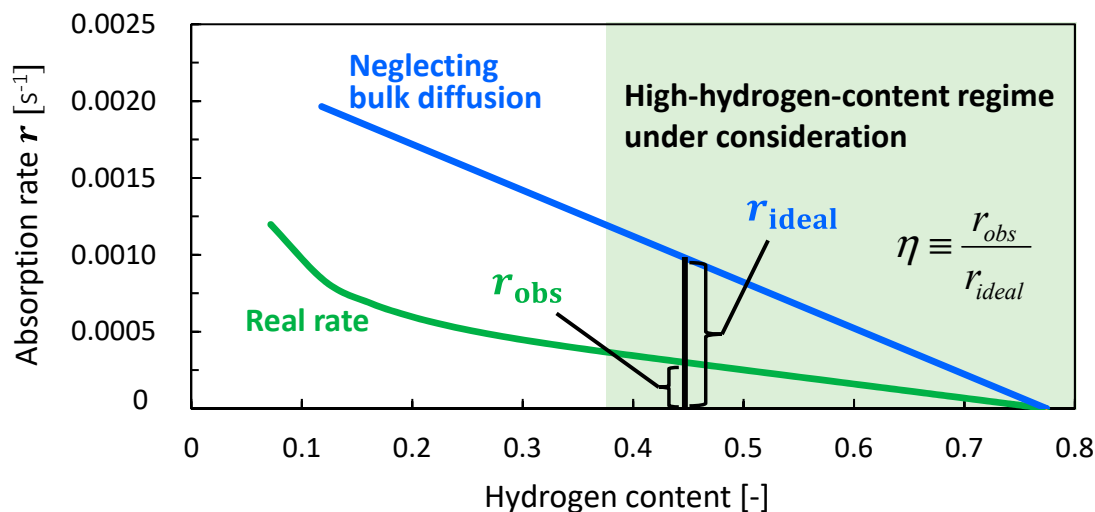

Figure 14. Conceptual schematic for definition of effectiveness factor η; $\eta = r_{obs}/r_{ideal}$, where r_{obs} and r_{ideal} are the actually observed hydrogen absorption rate that accounts for bulk diffusion and the virtual absorption rate that was calculated neglecting the bulk diffusion process. r_{obs} and r_{ideal} were plotted against the hydrogen content.
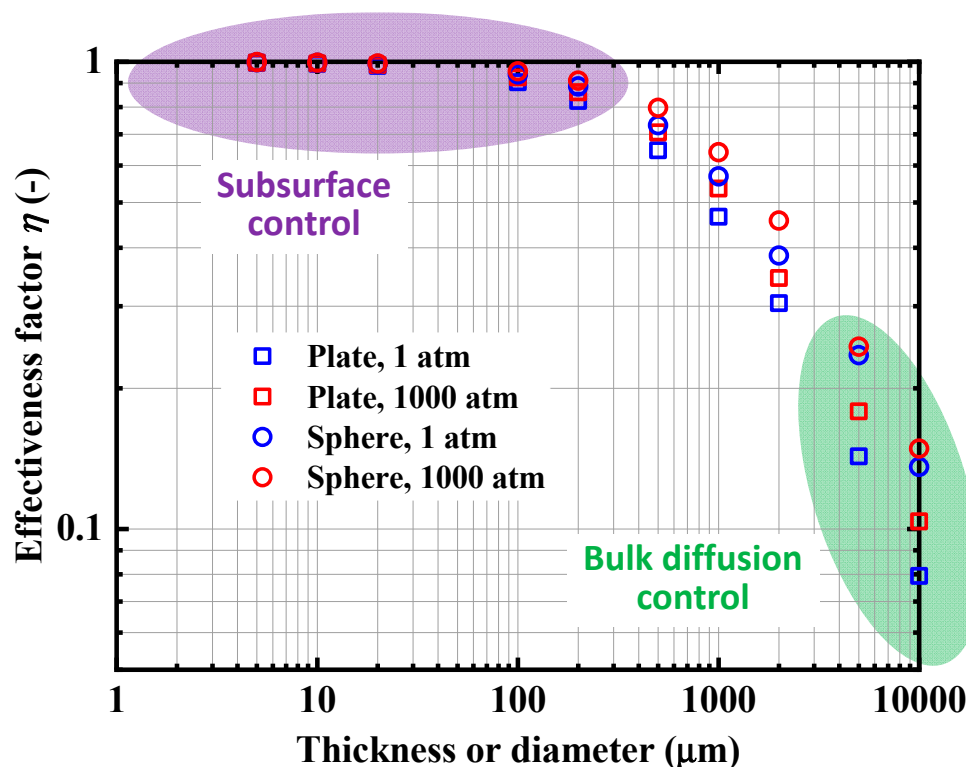

Figure 15. Calculated η values for Pd plates and spherical particles of various thicknesses and diameters, respectively, under constant hydrogen pressure of 1 and 1000 atm at 25 °C.

5. Conclusions

In this study, we developed a versatile kinetic numerical model for calculating the time-dependent rates of hydrogen absorption into metals. Our hydrogen transportation model particularly addressed the kinetics of the surface dissociative adsorption, subsurface transport (which significantly affects metals with active surfaces), and bulk diffusion. Moreover, this model enables us to perform flexible numerical simulations that could be universally used for various conditions, including different hydrogen absorbing material species, absorbing materials of different dimensions and structures, and, also, different operating conditions. Furthermore, our calculation scheme reflected the relationship between the temperature changes in metals, owing to the heat of adsorption and absorption, and the temperature-dependent kinetic parameters for highly precise numerical simulations. We demonstrated numerical calculations fitted a series of experimental data on hydrogen absorption for various Pd temperature ranges and sizes by a single set of the material's kinetic parameters. In another point of view, we have been able to finely extract the unknown kinetic parameters using a series of fittings. At the present stage, our numerical fitting was not necessarily excellent for the whole range of conditions. The fitting accuracy may be improved by increasing the precision of finely time-resolved pressure monitoring in the hydrogen absorption experiments. Nevertheless, the time constants for the absorption process were well reproduced for various Pd temperatures and sizes using a single set of modelling parameters. Using the developed model and the determined kinetic constants, the transitions of the rate-determining steps on the conditions of metal-hydrogen systems were systematically analyzed in a series of case studies. We showed the effectiveness of increasing the effective surface area, by several times relative to the smooth surface, to increase the hydrogen absorption rate for Pd through numerical simulations. Our simulation results also indicated that, to further increase the hydrogen absorption rate, it would be advantageous to decrease the influence of the bulk diffusion. Moreover, we found that decreasing the Pd size to 100 m would circumvent diffusion control for the kinetically efficient hydrogen absorption process. Conventionally, the changes in the temperature of metals during hydrogen adsorption and absorption have not been a favorable phenomenon because it could cause errors in the numerically estimated hydrogen absorption rates. By contrast, the model and numerical scheme we proposed in this study could represent highly accurate methods for determining unknown kinetic parameters, such as temperature-dependent rate constants, including the reaction activation energy, by numerically fitting the time-evolution experimental data of the hydrogen absorption rate. This would be similar to using the Arrhenius plot method; however, our model and scheme relies on a single experimental run as the temperature spontaneously varies owing to the exothermic adsorption and absorption processes. One can thus positively utilize the change in temperature of the hydrogen-absorbing media, to subsequently enable highly accurate numerical simulations. While we used Pd as the hydrogen-absorbing medium in this study, our numerical model could be applied to various types of metal/alloy-hydrogen systems. A potential disadvantage of our scheme may be the requirement of accurate monitoring of the time-transient temperature of the hydrogen-absorbing media, even for the temporal region with drastic temperature changes. In addition, we introduced an effectiveness factor: the ratio between the actual absorption rate and the virtually calculated one neglecting bulk diffusion, as a parameter that would allow us to evaluate the quantitative influence of each individual transport process and determine the rate-determining steps depending on the conditions of the metal-hydrogen systems, such as metal species and structures (e.g., sizes and shapes). The kinetic model and calculation scheme presented could allow for high-precision parameter determination and numerical simulations, and thus could be a useful tool for efficiently designing high-performance hydrogen storage systems.

Author Contributions: Y.H., Y.K., and K.T. conceived the idea of the study. E.Y. provided the experimental chamber and the Pd material. S.O., T.U., Y.H., Y.K., E.Y., and K.T. set up the experimental system. S.O., T.U., Y.H., Y.K., and G.Y. performed the experiments. S.O., T.U., Y.H., Y.K., and K.T. set up the theory. S.O., T.U., Y.H., and Y.K. carried out the calculations. S.O., T.U., Y.H., Y.K., G.Y., and K.T. analyzed the data. K.T. supervised the study. S.O., T.U., Y.H., and K.T. composed the manuscript.

References

1. Schlapbach, L.; Zuttel, A. Hydrogen-storage materials for mobile applications. *Nature* **2001**, *414*, 353–358. [CrossRef] [PubMed]

2. Ley, M.B.; Jepsen, L.H.; Lee, Y.S.; Cho, Y.W.; von Colbe, J.M.B.; Dornheim, M.; Rokni, M.; Jensen, J.O.; Sloth, M.; Filinchuk, Y.; et al. Complex hydrides for hydrogen storage—New perspectives. *Mater. Today* **2014**, *17*, 122–128. [CrossRef]

3. Mohtadi, R.; Orimo, S. The renaissance of hydrides as energy materials. *Nat. Rev. Mater.* **2016**, *2*, 16091. [CrossRef]

4. Behm, R.J.; Penka, V.; Cattania, M.G.; Christmann, K.; Ertl, G. Evidence for "subsurface" hydrogen on Pd(100): An intermediate between chemisorbed and dissolved species. *J. Chem. Phys.* **1983**, *78*, 7486–7490. [CrossRef]

5. Wilde, M.; Fukutani, K. Penetration mechanisms of surface-adsorbed hydrogen atoms into bulk metals: Experiment and model. *Phys. Rev. B* **2008**, *78*, 115411. [CrossRef]

6. Greeley, J.; Mavrikakis, M. Surface and subsurface hydrogen: Adsorption properties on transition metals and near-surface alloys. *J. Phys. Chem. B* **2005**, *109*, 3460–3471. [CrossRef]

7. Christmann, K. Interaction of hydrogen with solid surfaces. *Surf. Sci. Rep.* **1988**, *9*, 1–163. [CrossRef]

8. Dino, W.A.; Kasai, H.; Okiji, A. Orientational effects in dissociative adsorption/associative desorption dynamics of H_2 (D_2) on Cu and Pd. *Prog. Surf. Sci.* **2000**, *63*, 63–134. [CrossRef]

9. Pundt, A.; Kirchheim, R. Hydrogen in metals: Microstructural aspects. *Annu. Rev. Mater. Res.* **2006**, *36*, 555–608. [CrossRef]

10. Du, A.J.; Smith, S.C.; Yao, X.D.; Lu, G.Q. Hydrogen spillover mechanism on a Pd-doped Mg surface as revealed by ab initio density functional calculation. *J. Am. Chem. Soc.* **2007**, *129*, 10201–10204. [CrossRef]

11. Firmino, T.; Marquardt, R.; Gatti, F.; Dong, W. Diffusion rates for hydrogen on Pd(111) from molecular quantum dynamics calculations. *J. Phys. Chem. Lett.* **2014**, *5*, 4270–4274. [CrossRef] [PubMed]

12. Fukutani, K.; Wilde, M.; Ogura, S. Nuclear dynamics and electronic effects of hydrogen on solid surfaces. *Chem. Rec.* **2017**, *17*, 233–249. [CrossRef] [PubMed]

13. Lynch, J.F.; Flanagan, T.B. An investigation of the dynamic equilibrium between chemisorbed and absorbed hydrogen in the palladium/hydrogen system. *J. Phys. Chem.* **1973**, *77*, 2628–2634. [CrossRef]

14. Conrad, H.; Ertl, G.; Latta, E.E. Adsorption of hydrogen on palladium single crystal surfaces. *Surf. Sci.* **1974**, *41*, 435–446. [CrossRef]

15. Wagner, S.; Pundt, A. Quasi-thermodynamic model on hydride formation in palladium-hydrogen thin films: Impact of elastic and microstructural constraints. *Int. J. Hydrogen Energy* **2016**, *41*, 2727–2738. [CrossRef]

16. Huot, J.; Liang, G.; Boily, S.; Van Neste, A.; Schulz, R. Structural study and hydrogen sorption kinetics of ball-milled magnesium hydride. *J. Alloys Compd.* **1999**, *293*, 495–500. [CrossRef]

17. Pozzo, M.; Alfe, D. Hydrogen dissociation and diffusion on transition metal (= Ti, Zr, V, Fe, Ru, Co, Rh, Ni, Pd, Cu, Ag)-doped Mg(0001) surfaces. *Int. J. Hydrogen Energy* **2009**, *34*, 1922–1930. [CrossRef]

18. Evard, E.; Gabis, I.; Yartys, V.A. Kinetics of hydrogen evolution from MgH_2: Experimental studies, mechanism and modelling. *Int. J. Hydrogen Energy* **2010**, *35*, 9060–9069. [CrossRef]

19. Ward, T.L.; Dao, T. Model of hydrogen permeation behavior in palladium membranes. *J. Membr. Sci.* **1999**, *153*, 211–231. [CrossRef]

20. Bhargav, A.; Jackson, G.S.; Ciora, R.J.; Liu, P.T.K. Model development and validation of hydrogen transport through supported palladium membranes. *J. Membr. Sci.* **2010**, *356*, 123–132. [CrossRef]

21. Behm, R.J.; Christmann, K.; Ertl, G. Adsorption of hydrogen on Pd(100). *Surf. Sci.* **1980**, *99*, 320–340. [CrossRef]

22. Ali-Khan, I.; Dietz, K.J.; Waelbroeck, F.G.; Wienhold, P. The rate of hydrogen release out of clean metallic surfaces. *J. Nucl. Mater.* **1978**, *76*, 337–343. [CrossRef]

23. Kitagawa, Y.; Tanabe, K. Development of a kinetic model of hydrogen absorption and desorption in magnesium and analysis of the rate-determining step. *Chem. Phys. Lett.* **2018**, *699*, 132–138. [CrossRef]

24. Tanabe, K. Modeling of hydrogen/deuterium dynamics and heat generation on palladium nanoparticles for hydrogen storage and solid-state nuclear fusion. *Heliyon* **2016**, *2*, e00057. [CrossRef]

25. Frieske, H.; Wicke, E. Magnetic susceptibility and equilibrium diagram of PdH_n. *Ber. Der Bunsen-Ges. Fur Phys. Chem.* **1973**, *77*, 48–52. [CrossRef]